Variation of Peripapillary Scleral Shape With Age

Tin A. Tun,[1,2] Xiaofei Wang,[2,3] Mani Baskaran,[1,4] Monisha E. Nongpiur,[1,4] Yih-Chung Tham,[1] Shamira A. Perera,[1,4] Nicholas G. Strouthidis,[1,5,6] Tin Aung,[1,4,7] Ching-Yu Cheng,[1,4,7] and Michaël J. A. Girard[1,2]

[1]Singapore Eye Research Institute and Singapore National Eye Centre, Singapore
[2]Ophthalmic Engineering & Innovation Laboratory, Department of Biomedical Engineering, National University of Singapore, Singapore
[3]Beijing Advanced Innovation Center for Biomedical Engineering, School of Biological Science and Medical Engineering, Beihang University, Beijing, China
[4]Duke-NUS Medical School, Singapore
[5]NIHR Biomedical Research Centre, Moorfields Eye Hospital NHS Foundation Trust and UCL Institute of Ophthalmology, London, United Kingdom
[6]Discipline of Clinical Ophthalmology and Eye Health, University of Sydney, Sydney, New South Wales, Australia
[7]Department of Ophthalmology, Yong Loo Lin School of Medicine, National University of Singapore, Singapore

Correspondence: Michaël J. A. Girard, Ophthalmic Engineering & Innovation Laboratory (OEIL), Department of Biomedical Engineering, National University of Singapore, 4 Engineering Drive 3, E4-04-08, 117583, Singapore; mgirard@nus.edu.sg.

TAT and XW contributed equally to the work presented here and should therefore be regarded as equivalent authors.

Submitted: February 9, 2019
Accepted: June 18, 2019

Citation: Tun TA, Wang X, Baskaran M, et al. Variation of peripapillary scleral shape with age. *Invest Ophthalmol Vis Sci*. 2019;60:3275–3282. https://doi.org/10.1167/iovs.19-26777

Purpose. To define the shape of the anterior surface of the peripapillary sclera (PPS) and evaluate its relationship with age and ocular determinants in a population-based Chinese cohort.

Methods. The optic nerve heads of 619 healthy Chinese subjects were imaged with spectral-domain optical coherence tomography. To assess the shape of the PPS/Bruch's membrane (BM), we measured the angle between a line parallel to the nasal anterior PPS/BM boundary and one parallel to the temporal side. A negative value indicated that the PPS/BM followed an inverted v-shaped configuration (peak pointing toward the vitreous), whereas a positive value indicated that it followed a v-shaped configuration (peak pointing toward the orbital tissues). A linear regression model was used to evaluate the relationship between the PPS angle and other ocular parameters.

Results. The mean PPS angle was 3.68° ± 6.73° and the BM angle was 9.69° ± 5.05°. The PPS angle increased on average by 0.233 deg/y. A v-shaped PPS was significantly associated with age ($\beta = 0.087$, $P = 0.004$), peripapillary choroidal thickness ($\beta = -0.479$, $P < 0.001$), lamina cribrosa depth ($\beta = 0.307$, $P < 0.001$), and BM angle ($\beta = 0.487$, $P < 0.001$) after adjusting for best corrected visual acuity, central corneal thickness, and axial length.

Conclusions. The anterior surface of PPS of an elderly adult population had a v-shaped configuration and was more pronounced with increasing age, thin peripapillary choroid, and a deep cup. Such a change in shape with age could have an impact on the biomechanical environment of the optic nerve head.

Keywords: peripapillary sclera, age, choroidal thickness, laminar depth

Glaucoma, the leading cause of irreversible vision loss,[1] is characterized by the loss of retinal nerve fiber layers, narrowing of neuroretinal rim, and cupping of the optic nerve head (ONH) including loss of prelaminar tissues and bowing of lamina cribrosa (LC).[2,3] There is mounting evidence to suggest that the ONH and adjacent tissues are exposed to many mechanical loads such as intraocular pressure (IOP),[2,4] cerebrospinal fluid pressure (CSFP),[5] central retinal artery blood pressure,[6] and optic nerve traction[7,8] in a complex and dynamic behavior.

Around the posterior foramen, the inner third of scleral fibers becomes the scleral flange that anchors to the LC by thick columns of the connective tissues with enlarged bases at the periphery.[9,10] Since the peripapillary sclera (PPS) is a mechanical boundary for the ONH in principle, the role of the PPS in ONH biomechanics has been studied with relevance to glaucoma. Computational[11–13] and ex vivo studies[14,15] have reported that the PPS significantly affects the deformation of the LC following acute IOP elevations. An ex vivo study with porcine eyes has reported that stiffening the PPS with glutaraldehyde reduces LC deformations.[16] Moreover, in vivo human studies[17–19] report that acute IOP elevations deform LC posteriorly or anteriorly depending on the size and stiffness of the scleral canal.

Although the biomechanics of the PPS has been studied ex vivo extensively, studies on the scleral morphology adjacent to the ONH are lacking, especially in vivo. The morphology, thickness, and material properties of the PPS may be important for glaucoma pathophysiology,[20–22] but the thickness, morphology, and shape of the PPS in living human eyes have been difficult to assess and quantify owing to limitations in technology.

With advances in optical coherence tomography (OCT) technology, it is now possible to visualize the sclera or the interface between the sclera and choroid.[23–25] Sibony et al.[26] report that Bruch's membrane (BM) in healthy adults is a v-

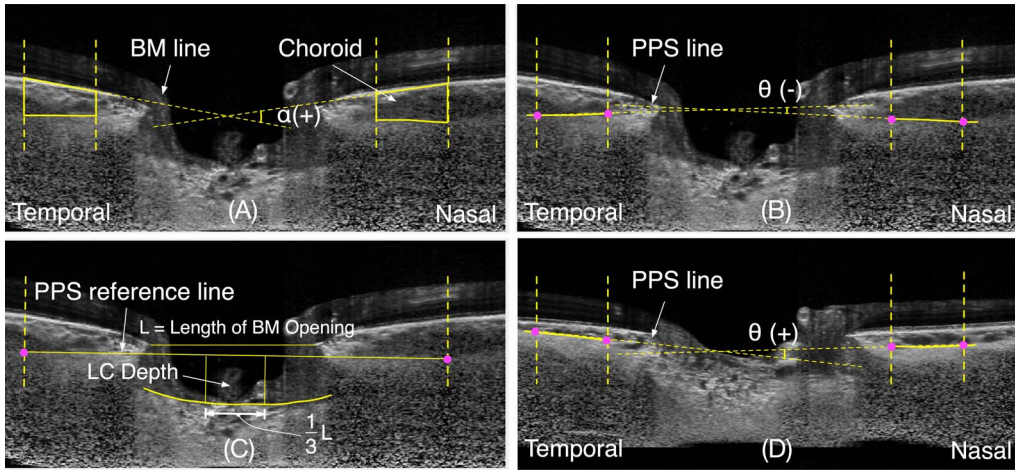

Figure 1. Illustration of measurement of Bruch's membrane angle and of the peripapillary scleral angle. (**A**) Illustration of a v-shaped Bruch's membrane angle, α; (**B**) Illustration of an inverted-v shaped PPS angle, θ(–); (**C**) The measurement of the depth of anterior surface of the lamina cribrosa (LC depth) from the peripapillary sclera reference plane; (**D**) Illustration of a v-shaped PPS angle, θ(+).

shaped configuration with its peak pointing toward the orbital tissues but they have not assessed the PPS. In this study, we aimed to define the shape of the PPS quantitatively, and how it is affected by age and other clinical/ocular parameters.

Methods

Subject Recruitment

Subjects were identified from the Singapore Chinese Eye Study (SCES), a population-based cohort study of ethnic Chinese subjects, aged 40 to 80 years, residing in southwestern Singapore. The recruitment protocol and study design of the SCES have been reported in detail.[27] In brief, the SCES was conducted to detect the prevalence and impact of major eye diseases among Chinese in Singapore. From 6350 names, an eligibility rate of 70% and a response rate of 75% were assumed to obtain the estimated target sample size of 3300 subjects with an age-stratified random sampling method.

A total of 3353 Chinese adults (72.8% response rate) participated in SCES1 and 2661 adults (87.7% response rate) attended in SCES2 after 6 years. The right eyes of 648 consecutive participants from SCES2 were analyzed in this substudy. Written informed consent was obtained from all participants. The study had the approval of the institutional review board of the SingHealth Centralized Institutional Review Board and adhered to the tenets of the Declaration of Helsinki.

Exclusion Case Definition

We excluded subjects defined as glaucoma or glaucoma suspects from the study. Glaucoma suspects were defined as those fulfilling any of the following criteria: (1) IOP $>$ 21 mm Hg, (2) vertical cup to disc ratio (VCDR) $>$ 0.6 or VCDR asymmetry $>$ 0.2, (3) abnormal anterior segment deposit consistent with pseudoexfoliation or pigment dispersion syndrome, (4) narrow anterior chamber angle (posterior trabecular meshwork is not seen in $\geq$2 quadrants by dark room gonioscopy), and (5) peripheral anterior synechiae.

Glaucoma cases were defined by the presence of glaucomatous optic neuropathy, defined as VCDR of $>$0.7 and/or neuroretinal rim narrowing with an associated visual field defect. The latter was defined if the following were found: (1) glaucoma hemifield test outside normal limits, (2) a cluster of $\geq$3, nonedge, contiguous points on the pattern deviation plot, not crossing the horizontal meridian with a probability of $<$5% being present in age-matched normals (one of which was $<$1%) and (3) pattern standard deviation $<$ 0.05; these were repeatable on two separate occasions. Reliability criteria for visual field test were defined as $<$20% fixation losses, $<$33% false-negative error, and $<$33% false-positive error, as recommended by Humphrey Instruments, Inc. (Dublin, CA, USA).

Optical Coherence Tomography Imaging and Analysis

The ONH of each subject was imaged with enhanced depth imaging spectral-domain OCT (SD-OCT; Spectralis, Heidelberg Engineering, Germany). Each OCT volume scan consisted of 97 serial horizontal B-scans (30-μm distance between B-scans; 384 A-scans per B-scan; 20 B-scans averaging) that covered a rectangular area of 15° × 10° centered on the ONH.[18,19]

Raw OCT images were postprocessed and enhanced by using adaptive compensation to reduce blood vessel shadows and to improve the visibility of the LC and PPS.[28–30] For each eye, postprocessed OCT volumes were resampled to obtain a central B-scan in the fovea-disc direction with a reference to the subject-specific fovea axis (Supplementary Fig. S1) and the central B-scan was analyzed with custom-written MATLAB (MathWorks, Inc., Natick, MA, USA) algorithms.

The position of the anterior LC and PPS was defined by a sharp increase in axial signal intensity extending laterally from the PPS to the LC through the LC insertion points.[31] Bruch's membrane opening (BMO) was defined as the end point of the BM layer (or the retinal pigment epithelium/BM complex) on either side of the ONH.[32] BMO was manually marked and a peripapillary ring was drawn from the center of BMO with the inner and outer radius of 1200 μm and 1800 μm, respectively.[33] The anterior surface of the PPS and BM within the ring were then manually delineated. The anterior surface of LC was also manually delineated (Fig. 1).

Using the aforementioned delineations, our custom algorithms derived the following parameters.[18,19]

Bruch's Membrane Angle (BM Angle). The BM angle was defined as an angle between a line parallel to the nasal BM and one parallel to the temporal BM. A negative value indicates that the anterior BM surface follows an inverted v-shaped configuration (peak pointing toward the vitreous), whereas a

Table 1. Demographic and Ocular Characteristics of the 619 Study Subjects

Characteristics	Mean (SD) or *n* (%)
Age, y	60.23 (7.36)
Sex, male	325 (52.5%)
Best corrected visual acuity, unit	0.11 (0.11)
Spherical equivalent, diopter	−0.21 (2.38)
Intraocular pressure, mm Hg	14.47 (2.4)
Central corneal thickness, μm	554.54 (32.65)
Anterior chamber depth, mm	3.36 (0.36)
Axial length, mm	24.05 (1.24)
Average corneal curvature, mm	7.65 (0.27)
Retinal nerve fiber layer thickness, μm	98.1 (10.08)
Choroidal thickness, μm	158.4 (53.98)
Lamina cribrosa depth, μm	363.65 (95.36)
Bruch's membrane angle, deg	9.69 (5.05)
Peripapillary scleral angle, deg	3.68 (6.73)

positive value indicates that it follows a v-shaped configuration (peak pointing toward the orbital tissues) (Fig. 1A).

Peripapillary Scleral Angle (PPS Angle). The PPS angle was defined as the angle between a line parallel to the nasal side of the anterior boundary of the sclera and another line parallel to the temporal side. As for BM, a negative value denotes an inverted v-shaped configuration of the PPS, while a positive value indicates a v-shaped configuration (Figs. 1B, 1D). Possible configurations of peripapillary scleral shapes, with corresponding angles, are illustrated in Supplementary Figure S2.

Lamina Cribrosa Depth (LCD). The LCD was defined as the distance from each anterior LC point to the PPS reference plane line in the central one-third of the length of BMO. The PPS reference plane was defined as a line connecting the outermost points of the anterior surface of the PPS ring. The mean depth of all LC points on the anterior LC surface was reported as the mean LC depth (Fig. 1C).

Peripapillary Choroidal Thickness (ChT). The ChT was defined as the thickness between the BM and PPS boundaries within the peripapillary ring and represented as the mean thickness in micrometers (Fig. 1A).

Validation of Grading

Repeatability of the segmentation of the images was evaluated by performing intra- and interrepeatability tests on the measurements of the BM and PPS angles. A subset of 40 images was selected by using simple random sampling method and delineated by a single observer. The same observer repeated the image segmentation in a random order after a 2-week interval for intraobserver repeatability. A different observer delineated the same set of images in a random order for the interobserver repeatability.

Statistical Analysis

Statistical analyses were performed with SPSS statistics for Windows (version 19.0; IBM Corp, Armonk, NY, USA). Continuous variables were described with means and standard deviations. We used linear regression models to assess the relationship of the PPS angle and of the BM angle with their determinants. We used Bland-Altman analysis of MedCalc (Windows v14.12.0; Mariakerke, Belgium) to compare the inter- and intraobserver repeatability of segmentation. Statistical significance was set at $P < 0.05$.

Results

Demographic and Clinical Characteristics

Of the 648 healthy subjects, 619 subjects were included in the final analysis after excluding 29 subjects (4.48%) whose OCT images had poor scleral visibility. Table 1 shows the demographic and clinical characteristics of the study participants. Most subjects were male (325/619, 52.5%) with a mean age of 60.23 ± 7.36 years. The mean PPS angle was 3.68° ± 6.73°, and the BM angle was 9.69° ± 5.05°. The PPS angle increased on average by 0.233 deg/y.

Relationship of BM Angle and/or PPS Angle With Its Determinants

An increase in the v-shaped configuration of the BM angle was significantly associated with longer axial length (Axl) (β = 0.089, $P = 0.028$), greater ChT ($\beta = 0.295$, $P < 0.001$), deeper LCD ($\beta = 0.443$, $P < 0.001$), increased PPS angle ($\beta = 0.479$, P

Table 2. Linear Regression Models: Bruch's Membrane Angle With Its Determinants

	Univariable		Multivariable Model 1		Multivariable Model 2	
Variables	β	*P* Value	β	*P* Value	β	*P* Value
Age, y	−0.01	0.802	−0.022	0.61		
Sex, male	0.032	0.429	−0.001	0.986		
Best corrected visual acuity, unit	0	0.991				
Spherical equivalent, diopter	−0.066	0.11	0.052	0.322		
Intraocular pressure, mm Hg	0.011	0.776	0.006	0.874		
Central corneal thickness, μm	−0.058	0.148	−0.024	0.539		
Axial length, mm	0.089	**0.028**	0.19	**0.001**	0.17	**<0.001**
Anterior chamber depth, mm	0.004	0.92				
Average corneal curvature, mm	0.006	0.89				
Retinal nerve fiber layer thickness, μm	−0.13	**0.011**	−0.102	**0.014**	−0.09	**0.017**
Choroidal thickness, μm	0.295	**<0.001**	0.49	**<0.001**	0.497	**<0.001**
Lamina cribrosa depth, μm	0.443	**<0.001**	0.171	**<0.001**	0.167	**<0.001**
Peripapillary scleral angle, deg	0.479	**<0.001**	0.437	**<0.001**	0.444	**<0.001**

The variables that may influence the Bruch's membrane angle were included in the multivariable model 1, and the variables that were significant in the univariable analysis were included in model 2. Bold values indicate statistical significance.

Investigative Ophthalmology & Visual Science

Table 3. Linear Regression Model: Peripapillary Scleral Angle With Its Determinants

	Univariable		Multivariable Model 1		Multivariable Model 2	
Variables	**β**	***P* Value**	**β**	***P* Value**	**β**	***P* Value**
Age, y	0.254	**<0.001**	0.092	**0.003**	0.087	**0.004**
Sex, male	−0.003	0.945	−0.045	0.121		
Best corrected visual acuity, unit	0.135	**0.001**	0.042	0.143	0.042	0.148
Spherical equivalent, diopter	−0.052	0.21				
Intraocular pressure, mm Hg	−0.004	0.922				
Central corneal thickness, μm	−0.092	**0.022**	−0.014	0.607	−0.013	0.637
Axial length, mm	0.085	**0.036**	−0.027	0.375	−0.038	0.2
Anterior chamber depth, mm	0.016	0.692				
Average corneal curvature, mm	−0.049	0.228				
Retinal nerve fiber layer thickness, μm	−0.066	0.2				
Choroidal thickness, μm	−0.305	**<0.001**	−0.475	**<0.001**	−0.479	**<0.001**
Lamina cribrosa depth, μm	0.446	**<0.001**	0.313	**<0.001**	0.307	**<0.001**
Bruch's membrane angle, deg	0.479	**<0.001**	0.484	**<0.001**	0.487	**<0.001**

The variables that may influence the peripapillary scleral angle were included in the multivariable model 1, and the variables that were significant in the univariable analysis were included in model 2. Bold values indicate statistical significance.

< 0.001), and thinner retinal nerve fiber layer thickness (RNFL) ($\beta = -0.13$, $P = 0.011$) (Table 2).

An increase in the v-shaped configuration of the PPS angle was also significantly associated with increasing age ($\beta = 0.254$, $P < 0.001$), poorer best corrected visual acuity (BCVA) ($\beta = 0.135$, $P = 0.001$), longer Axl ($\beta = 0.085$, $P = 0.036$), deeper LCD ($\beta = 0.446$, $P < 0.001$), increasing BM angle ($\beta = 0.479$, $P < 0.001$), thinner central corneal thickness (CCT) ($\beta = -0.092$, $P = 0.022$), and reduction in ChT ($\beta = -0.305$, $P < 0.001$) (Table 3).

Multivariable linear regression analysis showed that longer Axl ($\beta = 0.17$, $P < 0.001$), greater ChT ($\beta = 0.497$, $P < 0.001$), deeper anterior LC surface ($\beta = 0.167$, $P < 0.001$), thinner RNFL ($\beta = -0.09$, $P = 0.017$), and a v-shaped posterior sclera ($\beta = 0.444$, $P < 0.001$) were independently associated with a v-shaped BM configuration (Table 2).

A v-shaped PPS configuration was independently associated with increasing age ($\beta = 0.087$, $P = 0.004$), reduction in ChT ($\beta = -0.479$, $P < 0.001$), deeper LCD ($\beta = 0.307$, $P < 0.001$), and a v-shaped BM configuration ($\beta = 0.487$, $P < 0.001$) after adjusting for BCVA, CCT, and Axl (Table 3). A schematic, illustrating morphologic changes as a function of age and other clinical/demographic parameters, is shown in Figure 2.

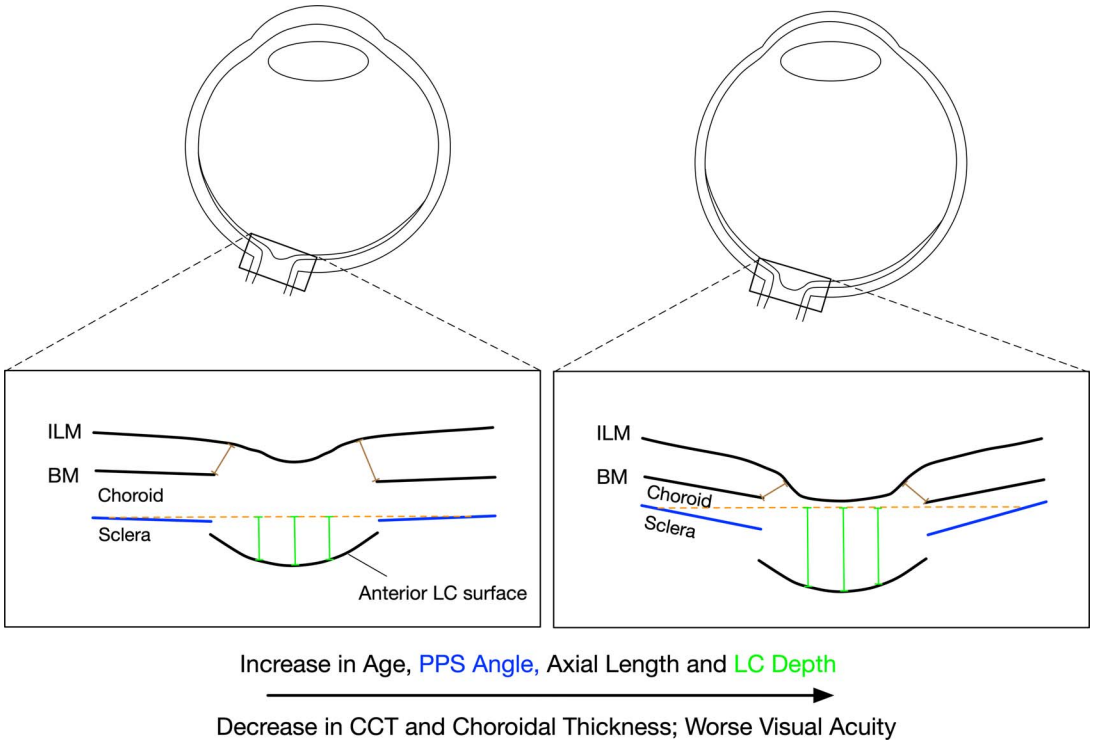

Figure 2. Illustration of the determinants of the peripapillary scleral angle in healthy eyes An increase in the v-shaped configuration of the PPS is associated with increasing age, longer axial length, thinner central corneal thickness, thinner peripapillary choroidal thickness, worse vision, and an increase in lamina cribrosa depth.

Investigative Ophthalmology & Visual Science

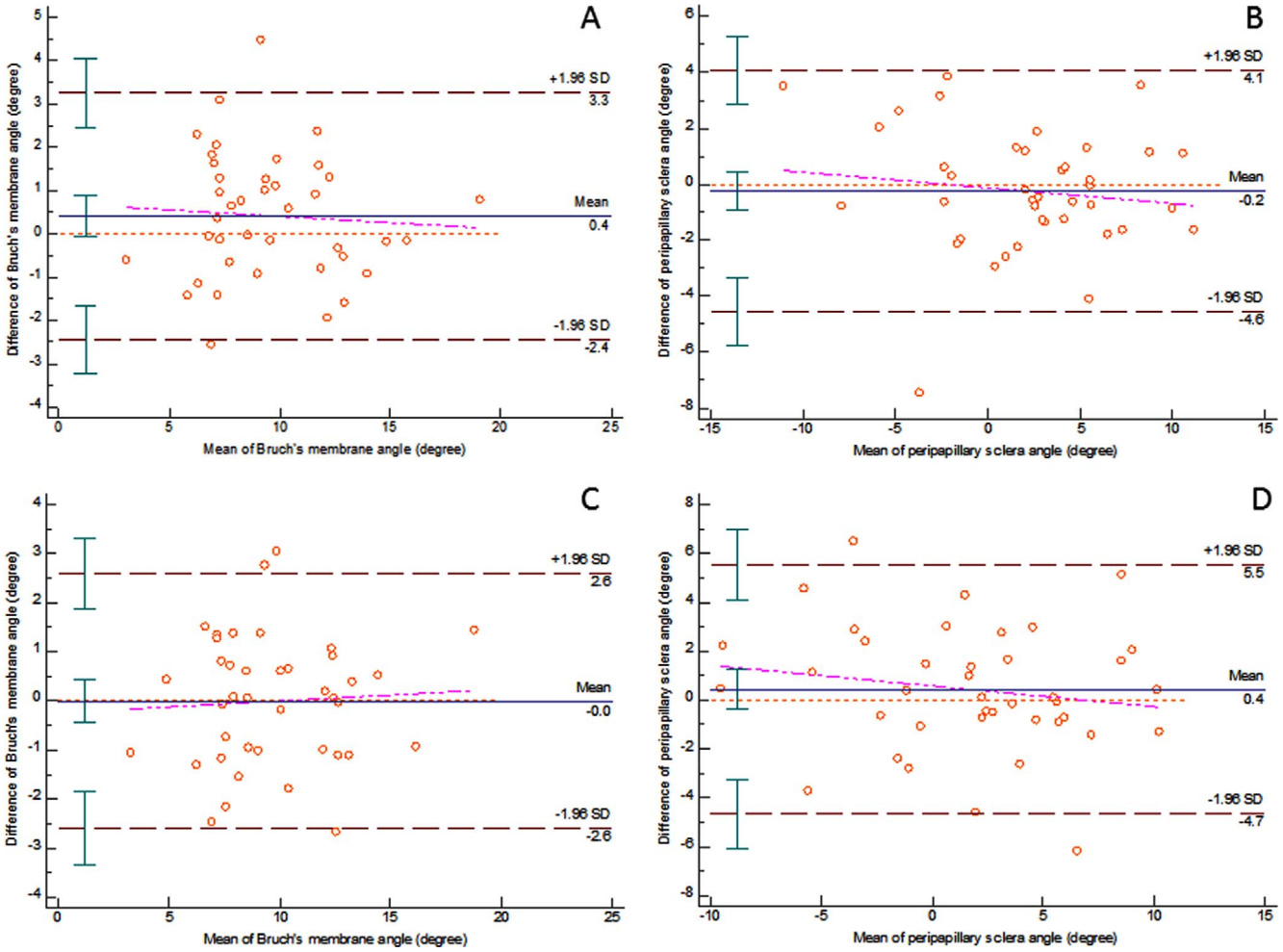

Figure 3. Bland-Altman plots of intra- and interobserver repeatability of image grading Intraobserver repeatability of image grading of Bruch's membrane angle (**A**) and the peripapillary scleral angle (**B**); interobserver repeatability of image grading of Bruch's membrane angle (**C**) and the peripapillary scleral angle (**D**) are illustrated. The *pink lines* represent the regression lines of differences and the *brown red lines* indicate the 95% confidence interval of limits of agreement.

Intra- and Interobserver Repeatability of Image Grading

Bland-Altman analysis of BM angle measurement showed that the mean difference was 0.413 (–0.051, 0.878, 95% confidence interval limit) for intraobserver repeatability and the mean difference was –0.003 (–0.428, 0.42, 95% confidence interval limit) for interobserver variability. The limits of agreement (LOA) for intraobserver variability was from –2.435 (–3.236, –1.634, 95% confidence interval limit) to 3.262 (2.461, 4.063, 95% confidence interval limit). The LOA for interobserver variability was from –2.601 (–3.331, –1.871, 95% confidence interval limit) to 2.593 (1.863, 3.323, 95% confidence interval limit) (Figs. 3A, 3C).

Bland-Altman analysis of PPS angle measurements showed that the mean difference was –0.242 (–0.946, 0.462, 95% confidence interval limit) for intraobserver repeatability and the mean difference was 0.436 (–0.396, 1.267, 95% confidence interval limit) for interobserver variability. The LOA for intraobserver variability was from –4.557 (–5.77, –3.343, 95% confidence interval limit) to 4.072 (2.859, 5.286, 95% confidence interval limit). The LOA for interobserver variability was from –4.662 (–6.095, –3.228, 95% confidence interval limit) to 5.533 (4.1, 6.967, 95% confidence interval limit) (Figs. 3B, 3D).

Discussion

In this study, we provided simple morphologic parameters to assess the shape of BM and of the anterior sclera in the peripapillary region through a single horizontal scan. This was performed in a cohort of healthy Chinese subjects. On average, the anterior surface of BM and of the PPS had a characteristic v-shaped configuration with its peak pointing toward the orbit. Their configurations ranged from an inverted v-shaped (but with relatively flat profile) to a more pronounced v-shaped configuration. For the PPS, the v-shaped configuration was more prominent with increasing age, worse vision, thinner cornea, greater axial length, thinner peripapillary choroid, and deeper anterior LC. Establishing and quantifying the morphology of the ONH could be critical in our understanding of ONH biomechanics.

The v-Shaped Configuration of the PPS Becomes More Pronounced With Age

In our study, we assessed the shape of the anterior sclera, an important load-bearing tissue of the eyes, and found that its shape was a characteristic v-shaped configuration in elderly Chinese eyes. The v-shaped configuration of the PPS (or the

obliqueness of the boundaries of the PPS) was more obvious with advancing age (Fig. 2). The reason for the v-shaped configuration in older adults is not exactly known. It is possibly due to the degeneration of ONH connective tissues (e.g., elastin) and thinning of the sclera[34,35] that occur in the course of aging. Furthermore, a reduction in CSFP after the age of 50 years[36] may play a role in age-related PPS changes. This reduction in CSFP may increase the translaminar pressure difference and may alter the PPS configuration in old age. Optic nerve traction forces generated throughout a lifetime of eye movements may be another possible influence. Studies[7,8,37] have shown that optic nerve traction during horizontal eye movements is able to pull the globe and deform the ONH. These traction forces may increase owing to age-related tissue stiffening (especially of the dura) and could affect the growth and remodelling of peripapillary tissues. This would result in a more v-shaped configuration in older subjects. Since the links between peripapillary tissue morphology and eye movements are still speculative, further studies are required to verify their potential relationships.

A more oblique PPS boundary was in general associated with a more oblique neural canal.[38] This oblique morphologic feature of the connective tissue in old age (which is the most common risk factor for glaucoma) may contribute to damage and posterior deformation when IOP increases in susceptible eyes. However, the clinical importance of these features and their usefulness in the management of glaucoma remain to be determined because the current study included only healthy eyes. Additionally, individual-specific changes in PPS shape with age could not be assessed in this study, and a longitudinal study is required to confirm our findings.

In additional to PPS shape, our results of BM shape are consistent with those of Sibony et al.[26] who report that the shape of BM in healthy eyes generally follows a v-shaped configuration.

The Shape of the PPS Is Associated With Other Ocular Factors

Histologic studies have shown that the sclera is the thinnest in the PPS region in monkeys[39] and humans.[40] Ren et al.[40] have reported that the thickness of PPS decreases significantly with increasing axial length, but its thickness is not different between glaucoma and control eyes. They therefore have hypothesized that the thickness of the PPS might not change remarkably in the process of glaucoma.[40] It is likely that the material properties and/or the shape of the PPS may be features that are remodelled in glaucoma pathogenesis.

In our study, we found that a more pronounced v-shaped configuration of the PPS was associated with a longer eyeball (increasing Axl) and a smaller CCT (Fig. 2). Unfortunately, owing to the limitations of OCT, we were not able to measure the thickness of the PPS. Imaging of this parameter might be possible with the development of longer-wavelength imaging techniques with deeper tissue penetration. We speculate that not only a thin sclera but also a pronounced v-shaped configuration may cause less resistance to mechanical insults of high IOP and play a role in glaucoma vulnerability.

We found that this v-shaped configuration of PPS was independently associated with a deeper cup of the ONH after adjusting for age, BCVA, ChT, CCT, and Axl. A large disc with a deep cup is thought to be more susceptible to pressure damage and may need to be monitored more closely.[41] Thus, an eye with a deep cup and a v-shaped PPS may be risk factors for glaucoma that need to be monitored closely. However, longitudinal studies are required to confirm such a hypothesis.

Tissue remodelling due to aging or disease alters not only the biomechanical properties of the ONH tissues but also their geometry (shape, thickness, and position) and the orientation of collagen fibers. Such changes will modify the biomechanical environment of the ONH, which could precipitate the progression of glaucoma. While techniques to assess the biomechanical properties and fiber orientation of ONH tissues in vivo are underway,[42–44] to date, only ONH morphology can be assessed clinically. Thus, we may consider morphologic parameters of ONH connective tissues, such as those proposed herein, for rapid clinical translation in order to better diagnose, risk profile, and ultimately manage glaucoma.

The strengths of the current study included a large population-based sample and a standardized study methodology. However, our study had a number of limitations. First, the population was exclusively Chinese, and our results may not be applicable to other ethnic groups. Second, only one B-scan was used to describe the 2-dimensional shape of the BM and of the PPS. Whilst this horizontal scan through the ONH was centered on the fovea to minimize any torsion, the horizontal area is not the one that changes very much in glaucoma. In fact, the areas where the double humps of the RNFL exist are the ones that change the most with glaucoma. Hence it might be more useful to target these areas in future. Alternatively, a 3-dimensional shape definition may be required. Third, limited visibility of the LC and of the PPS in some SD-OCT images weakened our methodology.

In summary, the anterior surface of the PPS in older adults followed a v-shaped configuration and was more pronounced with increasing age, thin peripapillary choroid, and a deep cup.

Acknowledgments

Supported by the Singapore Ministry of Education Academic Research Funds Tier 1 (R-397-000-294-114 [MJAG]) and Tier 2 (R-397-000-280-112 and R-397-000-308-114 [MJAG]), by Beijing Municipal Natural Science Foundation (7194288 [XW]), by the National Medical Research Council (NMRC/STAR/0023/2014 [TA]), and by the National Institute for Health Research (NIHR), Biomedical Research Centre, Moorfields Eye Hospital National Health Service (NHS), Foundation Trust and University College London, Institute of Ophthalmology (NGS). The sponsor or funding organization had no role in the design or conduct of this research. The views expressed are those of the author(s) and not necessarily those of the NHS, the NIHR, or the UK Department of Health.

Disclosure: **T.A. Tun**, None; **X. Wang**, None; **M. Baskaran**, None; **M.E. Nongpiur**, None; **Y.-C. Tham**, None; **S.A. Perera**, None; **N.G. Strouthidis**, None; **T. Aung**, None; **C.-Y. Cheng**, None; **M.J.A. Girard**, None

References

1. Quigley H, Broman AT. The number of people with glaucoma worldwide in 2010 and 2020. *Br J Ophthalmol*. 2006;90:262–267.
2. Weinreb RN, Aung T, Medeiros FA. The pathophysiology and treatment of glaucoma: a review. *JAMA*. 2014;311:1901–1911.
3. Quigley HA, Addicks EM, Green WR, Maumenee AE. Optic nerve damage in human glaucoma, II: the site of injury and susceptibility to damage. *Arch Ophthalmol*. 1981;99:635–649.
4. Sommer A. Intraocular pressure and glaucoma. *Am J Ophthalmol*. 1989;107:186–188.
5. Feola AJ, Coudrillier B, Mulvihill J, et al. Deformation of the lamina cribrosa and optic nerve due to changes in cerebrospinal fluid pressure. *Invest Ophthalmol Vis Sci*. 2017;58:2070–2078.

6. Hua Y, Voorhees AP, Sigal IA. Cerebrospinal fluid pressure: revisiting factors influencing optic nerve head biomechanics. *Invest Ophthalmol Vis Sci*. 2018;59:154–165.
7. Wang X, Rumpel H, Lim WEH, et al. Finite element analysis predicts large optic nerve head strains during horizontal eye movements. *Invest Opthalmol Vis Sci*. 2016;57:2452–2462.
8. Wang X, Beotra MR, Tun TA, et al. In vivo 3-dimensional strain mapping confirms large optic nerve head deformations following horizontal eye movements. *Invest Opthalmol Vis Sci*. 2016;57:5825–5833.
9. Anderson DR. Ultrastructure of human and monkey lamina cribrosa and optic nerve head. *Arch Ophthalmol*. 1969;82: 800–814.
10. Hayreh SS. *Ischemic Optic Neuropathies*. Berlin, Heidelberg: Springer Berlin Heidelberg; 2011.
11. Sigal IA, Flanagan JG, Ethier CR. Factors influencing optic nerve head biomechanics. *Invest Ophthalmol Vis Sci*. 2005; 46:4189–4199.
12. Sigal IA, Flanagan JG, Tertinegg I, Ethier CR. Modeling individual-specific human optic nerve head biomechanics, part I: IOP-induced deformations and influence of geometry. *Biomech Model Mechanobiol*. 2009;8:85–98.
13. Coudrillier B, Boote C, Quigley HA, Nguyen TD. Scleral anisotropy and its effects on the mechanical response of the optic nerve head. *Biomech Model Mechanobiol*. 2013;12: 941–963.
14. Yang H, Downs JC, Sigal IA, Roberts MD, Thompson H, Burgoyne CF. Deformation of the normal monkey optic nerve head connective tissue after acute IOP elevation within 3-D histomorphometric reconstructions. *Invest Opthalmol Vis Sci*. 2009;50:5785.
15. Braunsmann C, Hammer CM, Rheinlaender J, Kruse FE, Schäffer TE, Schlötzer-Schrehardt U. Evaluation of lamina cribrosa and peripapillary sclera stiffness in pseudoexfoliation and normal eyes by atomic force microscopy. *Invest Ophthalmol Vis Sci*. 2012;53:2960–2967.
16. Coudrillier B, Campbell IC, Read AT, et al. Effects of peripapillary scleral stiffening on the deformation of the lamina cribrosa. *Invest Ophthalmol Vis Sci*. 2016;57:2666–2677.
17. Agoumi Y, Sharpe GP, Hutchison DM, Nicolela MT, Artes PH, Chauhan BC. Laminar and prelaminar tissue displacement during intraocular pressure elevation in glaucoma patients and healthy controls. *Ophthalmology*. 2011;118:52–59.
18. Tun TA, Thakku SG, Png O, et al. Shape changes of the anterior lamina cribrosa in normal, ocular hypertensive, and glaucomatous eyes following acute intraocular pressure elevation. *Invest Ophthalmol Vis Sci*. 2016;57:4869–4877.
19. Tun TA, Atalay E, Baskaran M, et al. Association of functional loss with the biomechanical response of the optic nerve head to acute transient intraocular pressure elevations. *JAMA Ophthalmol*. 2018;136:184–192.
20. Olsen TW, Aaberg SY, Geroski DH, Edelhauser HF. Human sclera: thickness and surface area. *Am J Ophthalmol*. 1998; 125:237–241.
21. Vurgese S, Panda-Jonas S, Jonas JB. Scleral thickness in human eyes. *PLoS One*. 2012;7:e29692.
22. Sigal IA. Interactions between geometry and mechanical properties on the optic nerve head. *Invest Ophthalmol Vis Sci*. 2009;50:2785–2795.
23. Hayashi M, Ito Y, Takahashi A, Kawano K, Terasaki H. Scleral thickness in highly myopic eyes measured by enhanced depth imaging optical coherence tomography. *Eye (Lond)*. 2013;27: 410–417.
24. Lim LS, Cheung G, Lee SY. Comparison of spectral domain and swept-source optical coherence tomography in pathological myopia. *Eye*. 2014;28:488–491.
25. Gupta P, Cheng C-Y, Cheung CMG, et al. Relationship of ocular and systemic factors to the visibility of choroidal-scleral interface using spectral domain optical coherence tomography. *Acta Ophthalmol*. 2016;94:e142–e149.
26. Sibony P, Kupersmith MJ, James Rohlf F. Shape analysis of the peripapillary RPE layer in papilledema and ischemic optic neuropathy. *Invest Ophthalmol Vis Sci*. 2011;52:7987–7995.
27. Lavanya R, Jeganathan VSE, Zheng Y, et al. Methodology of the Singapore Indian Chinese Cohort (SICC) eye study: quantifying ethnic variations in the epidemiology of eye diseases in Asians. *Ophthalmic Epidemiol*. 2009;16:325–336.
28. Girard MJA, Strouthidis NG, Ethier CR, Mari JM. Shadow removal and contrast enhancement in optical coherence tomography images of the human optic nerve head. *Invest Opthalmol Vis Sci*. 2011;52:7738–7748.
29. Mari JM, Strouthidis NG, Park SC, Girard MJA. Enhancement of lamina cribrosa visibility in optical coherence tomography images using adaptive compensation. *Invest Opthalmol Vis Sci*. 2013;54:2238–2247.
30. Girard MJA, Tun TA, Husain R, et al. Lamina cribrosa visibility using optical coherence tomography: comparison of devices and effects of image enhancement techniques. *Invest Ophthalmol Vis Sci*. 2015;56:865–874.
31. Strouthidis NG, Grimm J, Williams GA, Cull GA, Wilson DJ, Burgoyne CF. A comparison of optic nerve head morphology viewed by spectral domain optical coherence tomography and by serial histology. *Invest Ophthalmol Vis Sci*. 2010;51: 1464–1474.
32. Tun TA, Sun CH, Baskaran M, et al. Determinants of optical coherence tomography-derived minimum neuroretinal rim width in a normal Chinese population. *Invest Ophthalmol Vis Sci*. 2015;56:3337–3344.
33. Vianna JR, Lanoe VR, Quach J, et al. Serial changes in lamina cribrosa depth and neuroretinal parameters in glaucoma: impact of choroidal thickness. *Ophthalmology*. 2017;124: 1392–1402.
34. Coudrillier B, Tian J, Alexander S, Myers KM, Quigley HA, Nguyen TD. Biomechanics of the human posterior sclera: age- and glaucoma-related changes measured using inflation testing. *Invest Ophthalmol Vis Sci*. 2012;53:1714–1728.
35. Girard MJA, Suh JKF, Bottlang M, Burgoyne CF, Downs JC. Scleral biomechanics in the aging monkey eye. *Invest Ophthalmol Vis Sci*. 2009;50:5226–5237.
36. Fleischman D, Berdahl JP, Zaydlarova J, Stinnett S, Fautsch MP, Allingham RR. Cerebrospinal fluid pressure decreases with older age. *PLoS One*. 2012;7:e52664.
37. Wang X, Fisher LK, Milea D, Jonas JB, Girard MJA. Predictions of optic nerve traction forces and peripapillary tissue stresses following horizontal eye movements. *Invest Opthalmol Vis Sci*. 2017;58:2044–2053.
38. Yang H, Downs JC, Bellezza A, Thompson H, Burgoyne CF. 3-D histomorphometry of the normal and early glaucomatous monkey optic nerve head: prelaminar neural tissues and cupping. *Invest Ophthalmol Vis Sci*. 2007;48:5068–5084.
39. Downs JC, Blidner RA, Bellezza AJ, Thompson HW, Hart RT, Burgoyne CF. Peripapillary scleral thickness in perfusion-fixed normal monkey eyes. *Invest Ophthalmol Vis Sci*. 2002;43: 2229–2235.
40. Ren R, Wang N, Li B, et al. Lamina cribrosa and peripapillary sclera histomorphometry in normal and advanced glaucomatous chinese eyes with various axial length. *Invest Ophthalmol Vis Sci*. 2009;50:2175–2184.
41. Hoffmann EM, Zangwill LM, Crowston JG, Weinreb RN. Optic disk size and glaucoma. Available at: https://www.ncbi.nlm.nih.gov/pmc/articles/PMC1850981/pdf/nihms17484.pdf. Accessed May 11, 2018.
42. Sigal IA, Grimm JL, Schuman JS, Kagemann L, Ishikawa H, Wollstein G. A method to estimate biomechanics and

Investigative Ophthalmology & Visual Science

mechanical properties of optic nerve head tissues from parameters measurable using optical coherence tomography. *IEEE Trans Med Imaging*. 2014;33:1381–1389.

43. Beotra MR, Wang X, Tun TA, et al. In vivo three-dimensional lamina cribrosa strains in healthy, ocular hypertensive, and glaucoma eyes following acute intraocular pressure elevation. *Invest Opthalmol Vis Sci*. 2018;59:260–272.
44. Zhang L, Thakku SG, Beotra MR, et al. Verification of a virtual fields method to extract the mechanical properties of human optic nerve head tissues in vivo. *Biomech Model Mechanobiol*. 2017;16:871–887.

Investigative Ophthalmology & Visual Science